Towards High Performance Finite Temperature Atomic Raman Quantum Memory: Analytical and Numerical Techniques

Journal of Physics: Conference Series **3183** (2026) 012002 doi:10.1088/1742-6596/3183/1/012002

Towards High Performance Finite Temperature Atomic Raman Quantum Memory: Analytical and Numerical Techniques

CHR Ooi[1] **and S Subramaniam**[1]

Abstract. *Quantum communication is an emerging field of the utmost importance. A critical component for scalable quantum communication, and other emerging quantum technologies is a robust practical quantum memory. We look at a theoretical model of a three level Λ quantum memory in a warm atomic gas complete with the Doppler broadening. A linearization procedure to compute solutions for the full set of Heisenberg-Langevin equations with the propagation equations is described. The atomic frequency comb (AFC) protocol together with the piecewise adiabatic passage (PAP) method in warm atomic gas is briefly discussed.*

[1] Department of Physics, Faculty of Science, Universiti Malaya, Kuala Lumpur, Malaysia.
Contact Phone: +60169632460

E-mail: rooi@um.edu.my

1. Introduction

A practical and reliable quantum memory (QM) is important for use in various quantum technologies, particularly for secure quantum communication. While there are schemes which use cascade configurations such as off-resonant cascaded configuration, the most commonly explored three-level configuration for QM is the lambda configuration. QM schemes such as electromagnetically induced transparency (EIT) [1, 2] and far-off resonance Raman memory (FORRM) [3], and also the three-level versions of controlled reversible inhomogeneous broadening (CRIB) [4, 5], gradient-echo memory (GEM) [6, 7, 8] and atomic frequency comb (AFC) [9, 10] use the lambda configuration, where one transition from a ground to an excited state is coupled with a weak quantum signal, and the other with a control laser field.

Pulse propagation in two-level system has been solved including noise operator using quantum Langevin [11] and wavefunction approach [12]. Full numerical solutions with spatial temporal propagation in 3 level medium has been developed [13]. For developing quantum information technology, proper quantum theory to describe quantum pulse is necessary.

In a previous work [14], we found a more general theory and analytical solution than that presented by Raymer [15] for stimulated Raman scattering (SRS). We have extended the analytical quantum field solution to include nonlocal linear response. Our solution is valid for both near resonance and far-off resonance, and also includes the AC Stark effect which was neglected in [15]. However, the solution did not include inhomogeneous broadening, and population dynamics, which are essential for QM schemes such as CRIB, GEM and AFC.

In this work we include population dynamics, **ac Stark shift** and the inhomogeneous broadening. We show that a linearization procedure **can lead to** hybrid analytical-numerical

approach for solving the Heisenberg-Langevin equations together with the propagation equation. We focus mainly on implementations in gases where the dominant inhomogeneous broadening is due to Doppler broadening. The formation of the AFC is simulated using the method in [16], which is then **used to simulate the storage and retrieval** of AFC quantum memory in a warm atomic gas.

2. Linearization Procedure to Solve the Heisenberg-Langevin Equations

The Heisenberg-Langevin equations for a closed-loop Λ-system (*shown in Fig. 1a*) is as follows:

$$\begin{aligned}
\frac{\partial\hat{\sigma}_{11}}{\partial t} &= 2\gamma_{31}\hat{\sigma}_{33} - i\left[\Omega_c\hat{\sigma}_{31} - \Omega_c^*\hat{\sigma}_{13}\right] f_c(z) + i\left[\Omega_m^* e^{i\phi}\hat{\sigma}_{12} - \Omega_m e^{-i\phi}\hat{\sigma}_{21}\right] f_m(z) + \hat{F}_{11} \quad (1)\\
\frac{\partial\hat{\sigma}_{22}}{\partial t} &= 2\gamma_{32}\hat{\sigma}_{33} + i\left[\Omega_m e^{-i\phi}\hat{\sigma}_{21} - \Omega_m^* e^{i\phi}\hat{\sigma}_{12}\right] f_m(z) - \frac{i}{\hbar}\wp_{13}\left[\hat{E}_s\hat{\sigma}_{32} - \hat{E}_s^\dagger\hat{\sigma}_{23}\right] + \hat{F}_{22}\\
\frac{\partial\hat{\sigma}_{33}}{\partial t} &= -2(\gamma_{31}+\gamma_{32})\hat{\sigma}_{33} + i\left[\Omega_c\hat{\sigma}_{31} - \Omega_c^*\hat{\sigma}_{13}\right] f_c(z) + \frac{i}{\hbar}\wp_{13}\left[\hat{E}_s\hat{\sigma}_{32} - \hat{E}_s^\dagger\hat{\sigma}_{23}\right] + \hat{F}_{33}\\
\frac{\partial\hat{\sigma}_{21}}{\partial t} &= (i(\Delta_s^u - \Delta_c^u) - \gamma_{21})\hat{\sigma}_{21} + i\Omega_m^* f_m(z)\, e^{i\phi}(\hat{\sigma}_{22} - \hat{\sigma}_{11}) + i\Omega_c^*\hat{\sigma}_{23} f_c(z) - \frac{i}{\hbar}\wp_{13}\hat{E}_s\hat{\sigma}_{31} + \hat{F}_{21}\\
\frac{\partial\hat{\sigma}_{31}}{\partial t} &= -(i\Delta_c^u + \gamma_{31} + \gamma_{32})\hat{\sigma}_{31} + i\Omega_c^*(\hat{\sigma}_{33} - \hat{\sigma}_{11}) f_c(z) - \frac{i}{\hbar}\wp_{13}\hat{E}_s^\dagger\hat{\sigma}_{21} + i\Omega_m^* f_m(z)\, e^{i\phi}\hat{\sigma}_{32} + \hat{F}_{31}\\
\frac{\partial\hat{\sigma}_{32}}{\partial t} &= -(i\Delta_s^u + \gamma_{31} + \gamma_{32})\hat{\sigma}_{32} + \frac{i}{\hbar}\wp_{13}\hat{E}_s^\dagger(\hat{\sigma}_{33} - \hat{\sigma}_{22}) - i\Omega_c^*\hat{\sigma}_{12} f_c(z) + i\Omega_m f_m(z)\, e^{-i\phi}\hat{\sigma}_{31} + \hat{F}_{32}
\end{aligned}$$

together with the propagation equation:

$$\left(\frac{\partial}{\partial z} + \varsigma_s\frac{1}{c}\frac{\partial}{\partial t}\right)\hat{E}_s(z,t) = i\beta\hat{\sigma}_{23}(z,t) \quad (2)$$

where $\Delta_s^u = \Delta_s - k_s u$, $\beta = \frac{\nu_p N}{2\epsilon_0 c}\wp_{13}$ and $\varsigma_s = \pm 1$ for forward and backward propagation respectively.

There are further potential benefits of optimizing QM performance using standing waves, using $f(z)$ as a dimensionless spatial function for the fields, and a train of pulses of the control field switched on, as in the case of dynamical decoupling scheme [17].

Together with their complex conjugates, these equations form a set of 11 partial differential equations which must be solved simultaneously. While the corresponding c-number equations can be solved easily using numerical methods (such as the 4th order Runge-Kutta method (RK4)), to solve the operator equations, we need a combined analytical and numerical method such as that in [18]. To be able to use this method, we need to perform the following linearization approximation:

$$\hat{E}\hat{\sigma}_{ij} = \frac{1}{2}\left(\mathcal{E}\hat{\sigma}_{ij} + \hat{E}S_{ij}\right) \quad (3)$$

where $\mathcal{E} = \left\langle\hat{E}\right\rangle$ and $S_{ij} = \langle\hat{\sigma}_{ij}\rangle$. We further need to discretize the z-derivative in the propagation equation Eq.(2) as follows:

$$\frac{1}{2}\frac{\partial}{\partial t}E_p(z+\Delta z,t) + \frac{1}{2}\frac{\partial}{\partial t}E_p(z,t) = ic\beta\hat{\sigma}_{23}(z,t) - \frac{\varsigma_s c}{\Delta z}\left[E_p(z+\Delta z,t) - E_p(z,t)\right] \quad (4)$$

Now we can write the system of differential equations in the following linear form:

$$\frac{d}{dt}\hat{Z}(z,t) = \mathbf{M}(z,t)\,\hat{Z}(z,t) + \mathbf{J}_z\hat{Z}(z-\Delta z,t) + \hat{F}(z,t) \quad (5)$$

The matrices $\mathbf{M}(z,t)$ and $\mathbf{J}_z = \frac{c\varsigma_s}{\Delta z}\begin{pmatrix} 0 & ... & 0 & 0 \\ ... & ... & 0 & 0 \\ 0 & 0 & 1 & 0 \\ 0 & 0 & 0 & 1 \end{pmatrix}$ are 11×11 matrices. Here $\hat{Z} = \left[\{\hat{\sigma}_{ij}\}, \hat{E}, \hat{E}^{\dagger}\right]^{\mathrm{T}}$ and $\hat{F} = \left[\{\hat{F}_{ij}\}, 0, 0\right]^{\mathrm{T}}$. In this paper, we use the convention that matrices are written in bold.

The formal solution is

$$\hat{Z}(z,t) = \mathbf{U}(z,t)\,\hat{Z}(z,0) + \int_0^t \mathbf{U}\left(z,t-t'\right)\left[\mathbf{J}_z\hat{Z}\left(z-\Delta z,t'\right) + \hat{F}\left(z,t'\right)\right]dt' \tag{6}$$

where

$$\mathbf{U}(z,t) = \prod_{i=0}^{t/\Delta t}\mathbf{u}(z,t) \tag{7}$$

$$\mathbf{u}(z,t) = \frac{\left(\mathbf{I} + \frac{\Delta t}{2}\mathbf{M}(z,t)\right)}{\left(\mathbf{I} - \frac{\Delta t}{2}\mathbf{M}(z,t)\right)} \tag{8}$$

which can be calculated numerically.

Solving the recurrence relation, we can find the general solution

$$\hat{Z}(z,t) = \sum_{n=0}^{N_z}\mathbf{K}_n(z,t)\,\hat{Z}(z-n\Delta z,0) + \int_0^t K_{N_z}\left(z,t-t'\right)\hat{Z}\left(0,t'\right)dt' + \sum_{n=0}^{N_z}\int_0^t K_n\left(z,t-t'\right)\hat{F}(z-n\Delta z,t\prime)\,dt' \tag{9}$$

where $\mathbf{K}_0 = \mathbf{I}$ and for $n \geq 1$

$$\mathbf{K}_n(z,t) = \int_0^t dt_1\mathbf{U}(z,t-t_1)\int_0^{t_1}dt_2\mathbf{J}_z\mathbf{U}(z-n\Delta z,t_2)\int_0^{t_2}dt_3...\int_0^{t_{n-1}}dt_n\mathbf{J}_z\mathbf{U}(z-n\Delta z,t_n) \tag{10}$$

This solution can be used to to calculate the efficiency and fidelity of a quantum memory scheme.

To include the Doppler broadening, we modify Eq. 4 as follows

$$\frac{\partial}{\partial t}E_p(z,t) = ic\beta\int_{-\infty}^{\infty}P(u)\,\hat{\sigma}_{23}(z,t,u)\,du - \frac{\varsigma_s c}{\Delta z}\left[E_p(z+\Delta z,t) - E_p(z,t)\right] \tag{11}$$

We can discretize the integration over velcoity u as follows:

$$\int P(u)\,\hat{\sigma}_{23}du \to \sum_{n=-N_u/2}^{N_u/2}P(n\Delta u)\,\hat{\sigma}_{23}(n\Delta u)\,\Delta u \tag{12}$$

Now instead of $\hat{Z}$ being a 11×1 vector, it has dimensions $(9N_u+2)\times 1$ with N_u being the total number of velocity points. $\mathbf{U}(z,t)$ now has dimensions $(9N_u+2)\times(9N_u+2)$ and the integration over u can be handled by matrix multiplication.

3. Preparation of AFC

In [16], a proposal using the piecewise adiabatic passage (PAP) technique to form an AFC was given, with a particular focus on Doppler broadened warm gases. The PAP method uses of a sequence of (**overlapping**) pump and dump pulses to transfer the populations between the

ground states in a Λ-system as shown in Fig. 1b, which was shown to be able to produce a comb shape distribution. In this section, we include the formulae that they have derived which are useful for comparison with the exact numerical simulation during the formation of an AFC. To minimize the effects of spontaneous emission, the two fields are far detuned $\Delta_0 \gg \Gamma$.

The density matrix equations for the system are are:

$$\begin{aligned}
\frac{\partial \rho_{11}}{\partial t} &= 2\gamma_{31}\rho_{33} - i\Omega_p\rho_{13} + i\Omega_p^*\rho_{31} \qquad (13a)\\
\frac{\partial \rho_{22}}{\partial t} &= 2\gamma_{32}\rho_{33} - i\Omega_d\rho_{23} + i\Omega_d^*\rho_{32}\\
\frac{\partial \rho_{33}}{\partial t} &= -2(\gamma_{31}+\gamma_{32})\rho_{33} + i\Omega_p\rho_{13} - i\Omega_p^*\rho_{31} + i\Omega_d\rho_{23} - i\Omega_d^*\rho_{32}\\
\frac{\partial \rho_{12}}{\partial t} &= (i(\Delta_d^u - \Delta_p^u) - \gamma_{21})\rho_{12} + i\Omega_p^*\rho_{32} - i\Omega_d\rho_{13}\\
\frac{\partial \rho_{13}}{\partial t} &= -(i\Delta_p^u + \gamma_{31} + \gamma_{32})\rho_{13} + i\Omega_p^*(\rho_{33} - \rho_{11}) - i\Omega_d^*\rho_{12}\\
\frac{\partial \rho_{23}}{\partial t} &= -(i\Delta_d^u + \gamma_{31} + \gamma_{32})\rho_{23} + i\Omega_d^*(\rho_{33} - \rho_{22}) - i\Omega_p^*\rho_{21}
\end{aligned}$$

Pump and dump pulses are modeled as ($f = p, d$)

$$\Omega_f = \Omega_{f0} e^{-\left(t-t_{f0}\right)^2/2T_e^2} \sum_{l=-N}^{N} e^{-\left(t-lT_{int}^f\right)^2/2T_f^2} \qquad (14)$$

which can transfer the population in the $|1\rangle$ state to the $|2\rangle$ state in a comb shape distribution. Here T_e is the envelope of the entire series of pulses. The parameters for AFC are computed according to the following chronology/sequence.

Spectral width due to Doppler broadening is $\Delta\nu_{\mathrm{FWHM}} = k_c \Delta u_{\mathrm{FWHM}} = \frac{2\pi}{\lambda_c} 2\sqrt{\frac{2k_B T}{m}\ln 2} = \sigma_e 2\sqrt{2\ln 2}$. We define N_c as the number of combs within the FWHM width $\Delta\nu_{\mathrm{FWHM}}$, $\Delta_{sep} = \frac{\Delta\nu_{\mathrm{FWHM}}}{N_c}$, or $\Delta\nu_{\mathrm{FWHM}} = N_c\Delta_{sep} = \sigma_e 2\sqrt{2\ln 2} \simeq 2.35\sigma_e$ equals **half** the base of the gaussian envelope .

Hence, we have the time between pulses T_{int} and pulse width T_P

$$T_{int} = \frac{2\pi\xi}{\Delta_{sep}} = \frac{2\pi N_c}{\Delta\nu_{\mathrm{FWHM}}}\xi \qquad (15)$$

$$T_P = \frac{T_{int}}{N_c} = \frac{2\pi}{\Delta\nu_{\mathrm{FWHM}}}\xi \qquad (16)$$

where the factor $\xi = \frac{k_c}{k_p - k_c}$ ensures the resolution of the peaks. For any T_{int} we use the factor ξ =54 (**corresponding to** $k_d = 0.98k_p$). If we use the numbers for Rb-87 D2 transitions [19] ξ would be very large the combs cannot be clearly depicted.

We verify that the Δ_{sep} from simulation correctly satisfies the equation $T_{int} = \frac{2\pi\xi}{\Delta_{sep}}$. Fixing the number of pulses N_p gives the envelope time $T_e = N_p T_{int}$.The number of combs can be expressed as $N_c = \frac{\Delta\nu_{\mathrm{FWHM}}}{\Delta_{sep}} = \frac{T_{int}}{T_P} = \frac{2\sqrt{2\ln 2}\sigma_e}{\Delta_{sep}}$. Using $T_{int} = \frac{2\pi N_c}{\sigma_e 2\sqrt{2\ln 2}}\xi = T_e/N_p$ we obtain

$$\xi = \frac{T_e\sigma_e}{N_p N_c}\frac{2\sqrt{2\ln 2}}{2\pi} \qquad (17)$$

The pulse spectral width (peak) σ_{pk} and finesse $\mathcal{F}$ can then be controlled by laser parameters as given by [16]

$$\sigma_{pk} = k_c u_{pk} = \frac{\sqrt{\pi}\Omega_0^2 T_P \xi}{4\Delta_0 T_{int}\sqrt{8\ln 2}} = \frac{\sqrt{\pi}\xi}{4\sqrt{8\ln 2}}\frac{\Omega_{ef}}{N_c} \tag{18}$$

$$\mathcal{F} = \frac{\Delta_{sep}}{\sigma_{pk}} = \frac{16\sqrt{\pi 2\ln 2}}{\Omega_{ef}T_P} = \frac{\Delta\nu_{\mathrm{FWHM}}8\sqrt{2\ln 2}}{\Omega_{ef}\xi\sqrt{\pi}} \tag{19}$$

where $\Omega_{ef} = \frac{\Omega_0^2}{\Delta_0}$ is the effective Rabi frequency.

We have developed a program to simulate the quantum dynamica; process by varying the parameters of the pump and dump pulses, and with this we see that Δ_{sep} matches our the predictions from the equations. In the simulations we set the decay rate to be $\Gamma = 3.8 \times 10^7 s^{-1}$ and the decoherences to be $\Gamma/2$. The detunings Δ_0 are set to 1000Γ satisfying $\Delta_0 \gg \Gamma$ and Ω_0 is set to give a peak width σ_{peak} smaller than Δ_{sep}, or $\Omega_{ef}T_P < 32$.

Population combs are produced when the pulses coincide and ramped (Fig. 3). For overlapping pulses (Fig. 4), the peaks are more symmetric. The order of pulses does not affect the outcome for both pulse orderings. The final time populations are the same even though the dynamics are different. While finite detuning is important to avoid populating the excited states, moderate detuning with sufficiently strong pulses are needed to establish significant (close to 1) population combs with regularly spaced peaks.

4. AFC Quantum Memory

One of the quantum memory schemes is the preparation of AFC before applying a laser pulse (c) to control the retrieve the quantum probe signal (s). In this section we discuss the characteristics of an AFC quantum memory as was first proposed by [9].

Given a comb distribution

$$P(u) = \frac{C}{\sqrt{2\pi}\sigma_{peak}} e^{-u^2/2u_e^2} \sum_{j=-N_c}^{N_c} e^{-(u-ju_{sep})^2/2u_{peak}^2} \tag{20}$$

where $C = \frac{1}{\sum_{j=-N_c}^{N_c} e^{-(j\Delta_{sep})^2/2\sigma_e^2}}$ is the required normalizing factor and the number of comb teeth is $2N_c + 1$. The comb parameters determine the performance of the quantum memory. The storage time is determined by peak separation:

$$\Delta_{sep} = \frac{2\pi}{T_{store}} \tag{21}$$

while the finesse of the comb is defined as $\mathcal{F} = \frac{\Delta_{sep}}{\sigma_{peak}}$ and is related to the efficiency of the quantum memory as shown below (note that in [9], in the definition of $\mathcal{F}$, the full-width-at-half-maximum (FWHM) values is used instead, and the expressions for efficiency should be modified accordingly).

The optical depth for the medium is defined as $d = \alpha L$ where L is the length of the medium, and the absorption coefficient

$$\alpha = C\frac{(2\pi)^2}{\Delta_{sep}}\beta\frac{\wp_{23}}{\hbar} = C\frac{(2\pi)^2}{\Delta_{sep}}\frac{N\nu_s\wp_{23}^2}{2\hbar\epsilon_0 c} \tag{22}$$

depends on the properties of the comb.

[9] obtained results for both the forward and backward protocol. They are
Forward Protocol:

$$E_f(L,t) = E_f(0, t - T_{store})\, d e^{-2\pi^2/F^2} e^{-d/2} \tag{23}$$

$$\eta_F = \frac{|E_f(L,t)|^2}{|E_f(0, t-\tau_S)|^2} = e^{-4\pi^2/F^2} d^2 e^{-d} \tag{24}$$

Backward Protocol:

$$E_b(0,t) = -E_f(0, t - T_{store}) \left[e^{-2\pi^2/F^2} \left(1 - e^{-d}\right)\right] \tag{25}$$

$$\eta_B = \frac{|E_b(0,t)|^2}{|E_f(0, t-T_{store})|^2} = e^{-4\pi^2/F^2} \left(1 - e^{-d}\right)^2 \tag{26}$$

where in general the efficiency of a quantum memory has been defined as $\eta = \frac{|E_{out}|^2}{|E_{in}|^2}$.

The periodic distribution produces a periodic rephasing which results in the an output pulse being reemitted after a time T_{store} which is inversely proportional to the separation between AFC peaks. We have developed a numerical simulation code using the RK4 algorithm that demonstrates the predicted rephasing. As shown in Fig. 5 for the forward protocol the efficiency agrees with analytical efficiency (when decoherence is neglected).

The pulse reaches maximum at around 0.5 and is reabsorbed by the medium before emerging from the medium with tiny amplitude. This shows that if the output boundary is right, coincides with the position where the retrieved pulse is at its peak, significant output signal can be retrieved.

$$\Omega_c(t) = \Omega_{c1} e^{-(t-t_{c1})^2/2T_{c1}^2} + \Omega_{c2} e^{-(t-t_{c2})^2/2T_{c2}^2} \tag{27}$$

When control pulse is present, the timing and efficiency of the signal can be controlled (Fig. 6). The efficiency is optimized when the first pulse coincides with the signal pulse ($t_{c1} = t_s$) is long and the the second pulse is short (but not too short as it will produce subsequent secondary signal, reducing the efficiency of primary signal). The second pulse can be delayed by time ($t_{c2} = t_{c1} + T_{store} + \kappa T_s$) before ($\kappa < 0$) or after ($\kappa > 0$) the storage time T_{store} and this is useful for adjusting the on-demand retrieval time, without much affecting the efficiency. Analyzing these plots leads to the use of a higher density to obtain peak efficiency above 85% (Fig. 5), and perfect efficiency is possible by using larger Ω_{c2}.

5. Discussion and Conclusions

The linearization procedure and semi-analytical solution that we have outlined may be used to compute the solutions to the full set of Heisenberg-Langevin equations together with the noise operator and provides a complete approach to model a quantum memory. We can include the Doppler broadening in warm atomic gases in the pursuit of a robust quantum memory protocol.

The AFC protocol by [9] is a promising approach for room temperature quantum memory. To study the implementation on warm atomic gases, we have developed the RK4 algorithm to simulate the memory with the full set of density matrix equations for a three-level Raman system together with the propagation equations for the fields. We have also simulated the PAP method outlined by [16], where the parameters for the comb generated match closely with the formulae given for zero decoherences.

These simulations are important in demonstrating the working principles of a AFC quantum memory. As expected, the periodic distribution in the AFC protocol results in re-emission of a signal pulse. We have also explored the effects of incorporating the control laser pulses into the protocol.

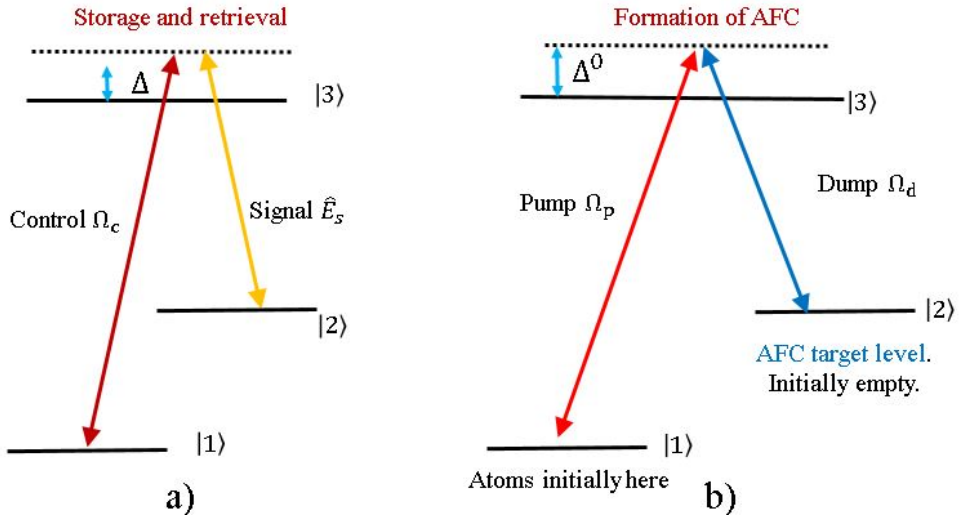

Figure 1. a) Level scheme for storage and retrieval of quantum signal pulse using control laser pulses. b) preparation of atomic frequency comb (AFC) in level 2 using pump and dump pulses.

Our simulations demonstrate very high retrieval efficiency, an important promising method of creating an AFC distribution in a warm atomic gas. For future research, we may consider robust methods for creating an AFC, and also the possibility of alternative distributions which may be simpler to produce, while having good performance in a quantum memory.

Acknowledgments

We acknowledge the support by Ministry of Higher Education (MOHE) Malaysia, under Long-Term Research Grant Scheme, LRGS/1/2020/UM/01/5/1. R Ooi thanks Dieter Suter for helpful discussions.

References

[1] Fleischhauer M and Lukin M D 2000 *Physical Review Letters* **84** 5094–5097 pRL URL https://link.aps.org/doi/10.1103/PhysRevLett.84.5094
[2] Fleischhauer M and Lukin M D 2002 *Physical Review A* **65** 022314 pRA URL https://link.aps.org/doi/10.1103/PhysRevA.65.022314
[3] Reim K F, Nunn J, Lorenz V O, Sussman B J, Lee K C, Langford N K, Jaksch D and Walmsley I A 2010 *Nature Photonics* **4** 218–221 ISSN 1749-4893 URL https://doi.org/10.1038/nphoton.2010.30
[4] Kraus B, Tittel W, Gisin N, Nilsson M, Kröll S and Cirac J I 2006 *Physical Review A* **73** 020302 pRA URL https://link.aps.org/doi/10.1103/PhysRevA.73.020302
[5] Sangouard N, Simon C, Afzelius M and Gisin N 2007 *Physical Review A* **75** 032327 pRA URL https://link.aps.org/doi/10.1103/PhysRevA.75.032327
[6] Alexander A L, Longdell J J, Sellars M J and Manson N B 2006 *Physical Review Letters* **96** 043602 pRL URL https://link.aps.org/doi/10.1103/PhysRevLett.96.043602
[7] Hétet G, Hosseini M, Sparkes B M, Oblak D, Lam P K and Buchler B C 2008 *Optics Letters* **33** 2323–2325 URL https://opg.optica.org/ol/abstract.cfm?URI=ol-33-20-2323
[8] Hétet G, Longdell J J, Alexander A L, Lam P K and Sellars M J 2008 *Physical Review Letters* **100** 023601 pRL URL https://link.aps.org/doi/10.1103/PhysRevLett.100.023601
[9] Afzelius M, Simon C, de Riedmatten H and Gisin N 2009 *Physical Review A* **79** 052329 pRA URL https://link.aps.org/doi/10.1103/PhysRevA.79.052329
[10] Afzelius M, Usmani I, Amari A, Lauritzen B, Walther A, Simon C, Sangouard N, Minář J, de Riedmatten H, Gisin N and Kröll S 2010 *Physical Review Letters* **104** 040503 pRL URL https://link.aps.org/doi/10.1103/PhysRevLett.104.040503
[11] Ooi C H R 2008 *Physical Review A* **77** 053820 pRA URL https://link.aps.org/doi/10.1103/PhysRevA.77.053820

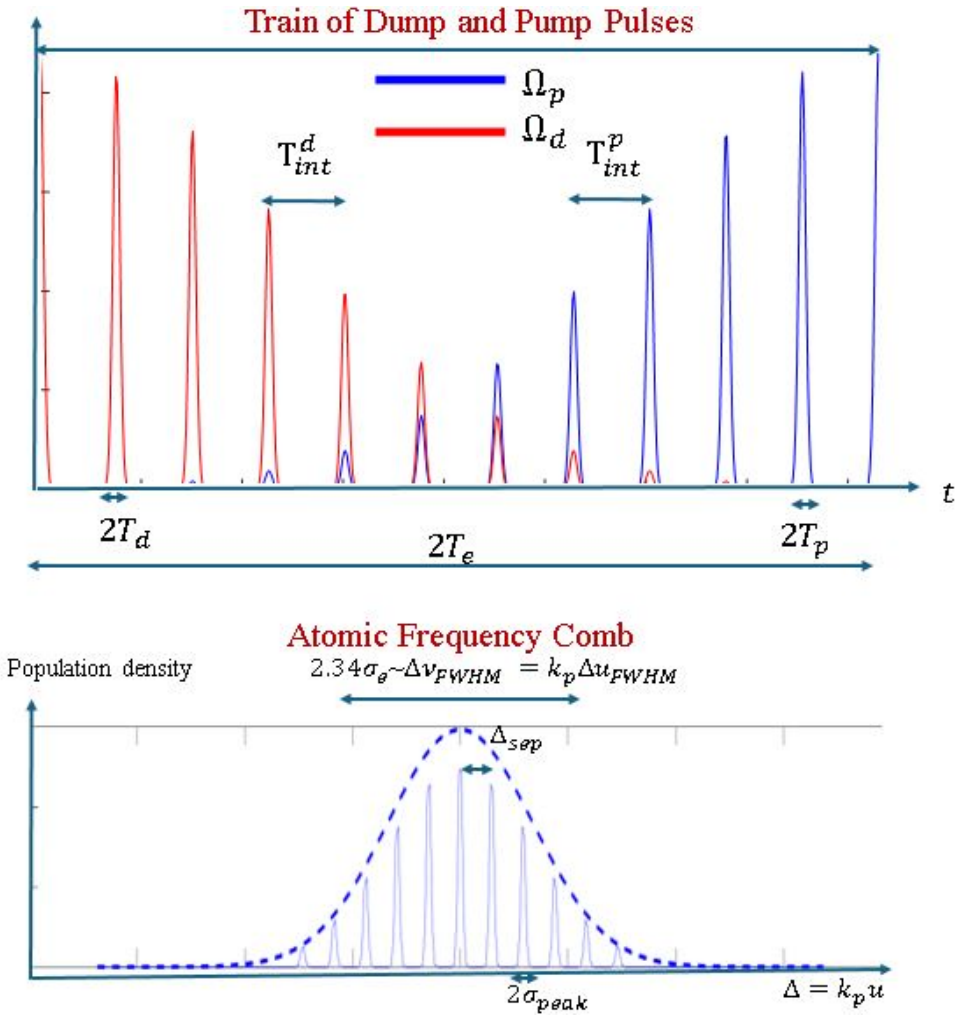

Figure 2. Temporal and spectral distributions of the pulses with defined widths.

[12] Berman P R and Ooi C H R 2011 *Physical Review A* **84** 063851 pRA URL https://link.aps.org/doi/10.1103/PhysRevA.84.063851
[13] Ooi C H R, Harun S W and Ahmad H 2011 *Journal of Modern Optics* **58** 11–13 ISSN 0950-0340 doi: 10.1080/09500340.2010.521594 URL https://doi.org/10.1080/09500340.2010.521594
[14] Shreyes S, Huang Y and Ooi C H R 2023 *Laser Physics* **33** 095201 ISSN 1555-6611 1054-660X URL https://dx.doi.org/10.1088/1555-6611/ace9cf
[15] Raymer M G and Mostowski J 1981 *Physical Review A* **24** 1980–1993 pRA URL https://link.aps.org/doi/10.1103/PhysRevA.24.1980
[16] Rubio J L, Viscor D, Mompart J and Ahufinger V 2018 *Physical Review A* **98** 043834 pRA URL https://link.aps.org/doi/10.1103/PhysRevA.98.043834
[17] Souza A M, Álvarez G A and Suter D 2011 *Phys. Rev. Lett.* **106**(24) 240501 URL https://link.aps.org/doi/10.1103/PhysRevLett.106.240501
[18] Ooi C H R 2011 *Physical Review A* **84** 053842 pRA URL https://link.aps.org/doi/10.1103/PhysRevA.84.053842
[19] A S D 2010 Alkali d line data (available at: http://steck.us/alkalidata)

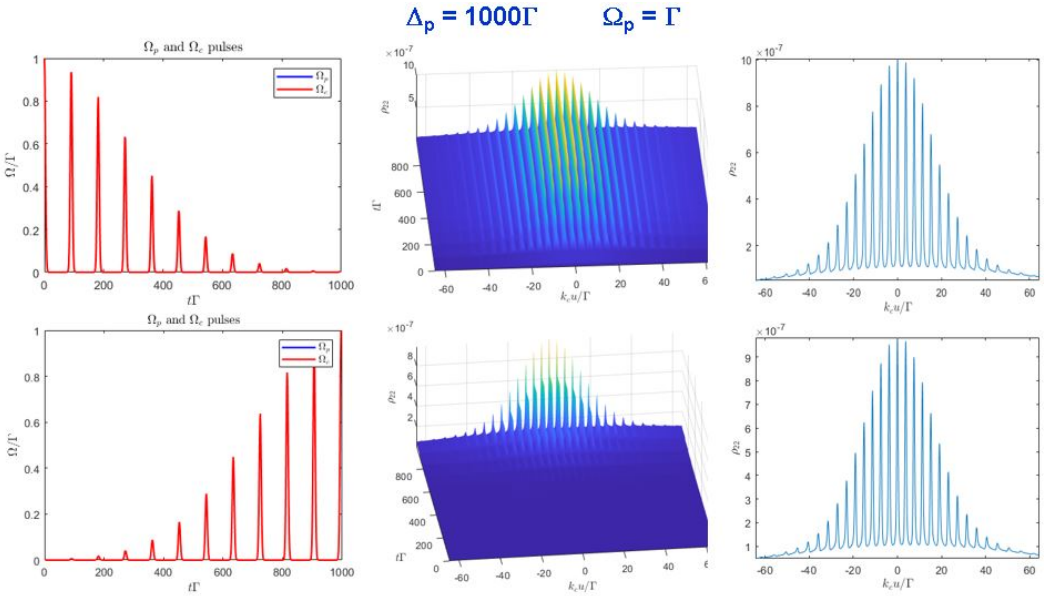

Figure 3. Atomic population-frequency comb for identical series of the pump and dump pulses

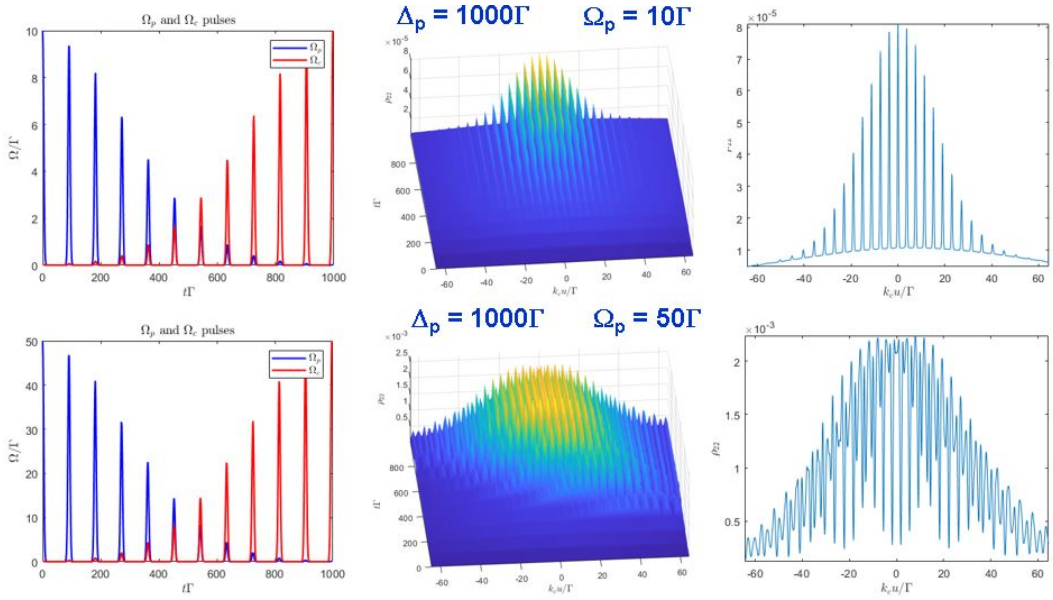

Figure 4. Atomic population-frequency comb for overlapping series of pump and dump pulses.

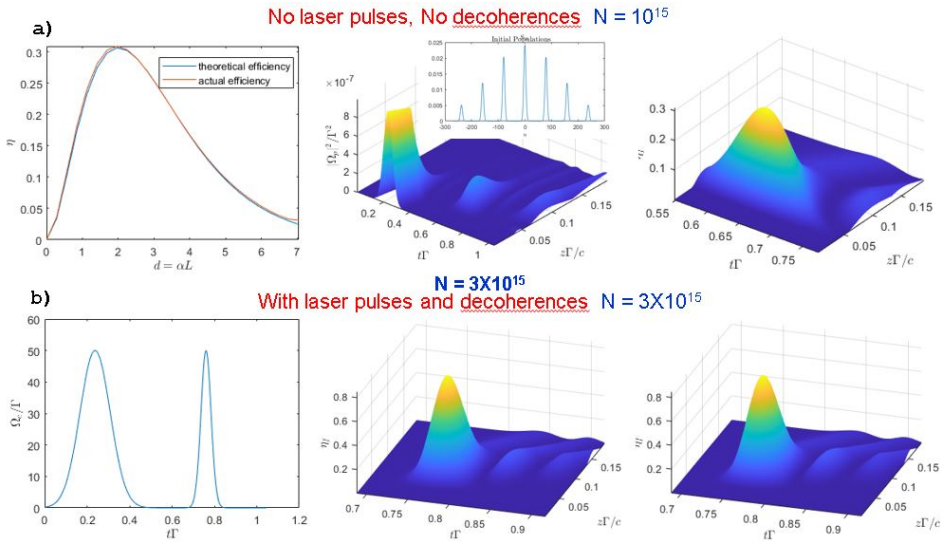

Figure 5. Spatial and temporal evolution of quantum (signal) pulse in AFC medium a) without control laser and without decoherence and dissipation, b) with control laser pulses, finite decoherence and dissipation. We use optimum parameters:$\Delta = 0, \kappa = 3, T_{store} = 3/c, N = 3 \times 10^{15} m^{-3}. T_s = T_{store}/8$, $T_{c1} = 1.5T_s; T_{c2} = \mathbf{0.5}T_s$ and $\Omega_{c1} = \Omega_{c2} = 50\Gamma, \Omega_s = \Gamma/10^3$.

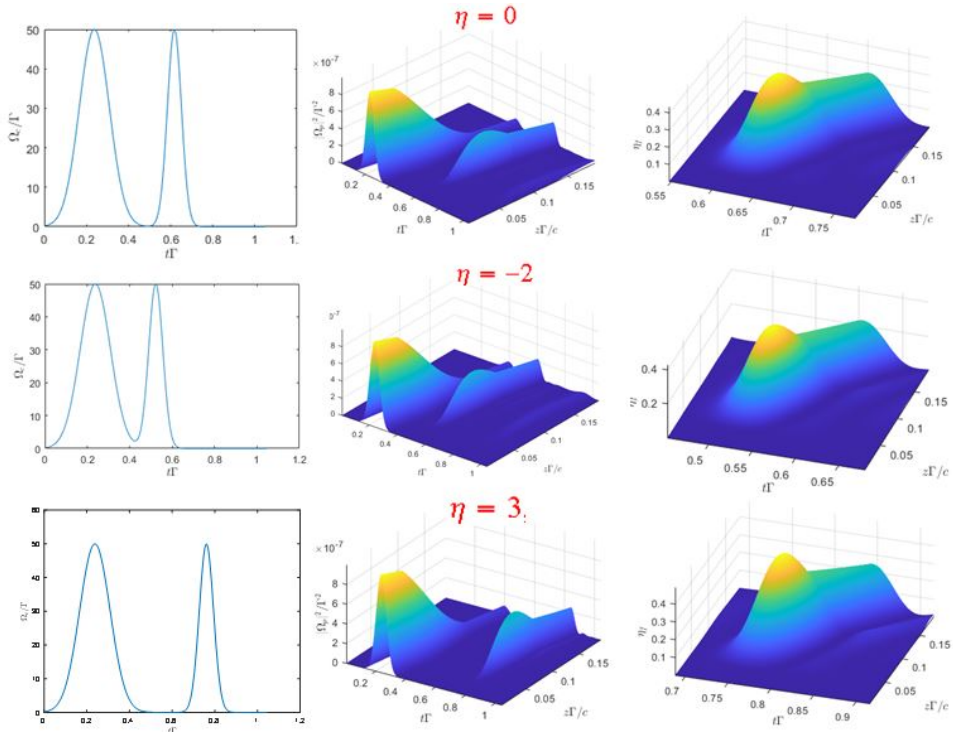

Figure 6. Spatial and temporal evolution of quantum (signal) pulse emerging from AFC medium with control laser pulses: $\Delta = 0, \kappa = 0, \kappa = -2, \kappa = 3$ with $T_{store} = 3/c$. Number density $N = 10^{15} m^{-3}$, storage time $3/c$. Decoherence and dissipation are included. We use: $T_s = T_{store}/8$, $T_{c1} = 1.5T_s, T_{c2} = 0.7T_s$ and $\Omega_{c1} = \Omega_{c2} = 50\Gamma, \Omega_s = \Gamma/10^3$.